NEW POSITRON SOURCE FOR CESR

J. Barley, V. Medjidzade, A. Mikhailichenko

Wilson Laboratory, Cornell University, Ithaca, NY 14853[∗]

Abstract

Some details of the new positron converter and power supply are described. This converter unit so far has doubled the amount of positrons accelerated in synchrotron.

1. INTRODUCTION

With the installation and testing of the new positron converter unit the first stage of improvement of this device is accomplished. This stage deals with the collection optics; i.e. elements located right after the target. It also includes the new power supply construction and testing. Other (possible) stages will include modifications of optics located *before* the target.

During last few years there have been investigations of both pre-target and post-target optics [1-6].

At the CESR complex a bi-layer solenoid was used as a short focusing lens, located right after the target. This lens provided a Quarter Wave Transformation (QWT) i.e. the target was located on a focal plane of this lens. This type of focusing system was originated in [6]. The target was located at the end of a paddle-type holder in front of this bi-layer coil.

In [5] it was shown that geometrical collection of positrons after the target could be increased, if the feeding current increased in a short focusing solenoidal lens.

On the other hand an attempt to increase the current identified the other problem concerning the symmetry of the field in general. As the field in the focusing coil increased, the transverse kick increased also. So the positive effect of focusing was diminished by the excitation of a transverse kick. This transverse kick was generated by the target holder as well as asymmetric surroundings around the coil [4], [5].

Meanwhile the requirement for positron accumulation in CESR at the minimal level 100 *mA/min* yielded a necessity for a new positron conversion unit. In this unit all accumulated knowledge about the system was to be used for reaching this goal and pave the road for further improvements.

As this job was successfully accomplished we represent here a general description of what was done on the way.

## 2. BASIC CONCEPTS OF NEW COLLECTION SYSTEM

Four basic principles of the new collection system are: **shorter focal distance** of the lens with its closer positioning to the target, the **possibility of alignment** of converter unit with respect to accelerating structure, the maximal possible **symmetrical allocation for input wires** and, last, but not least, **symmetry of the surroundings**.

First principle illustrated in Fig.2.1. The rear plane of the target coincides with the focal plane of the short focusing lens. As the scattering processes in the target media fixes the divergence of the

---

secondary beam, the shorter focal length allows smaller beam sizes. For some extent if there is no limitation in transverse size of the lens, this can allow an increase of capturing angle.
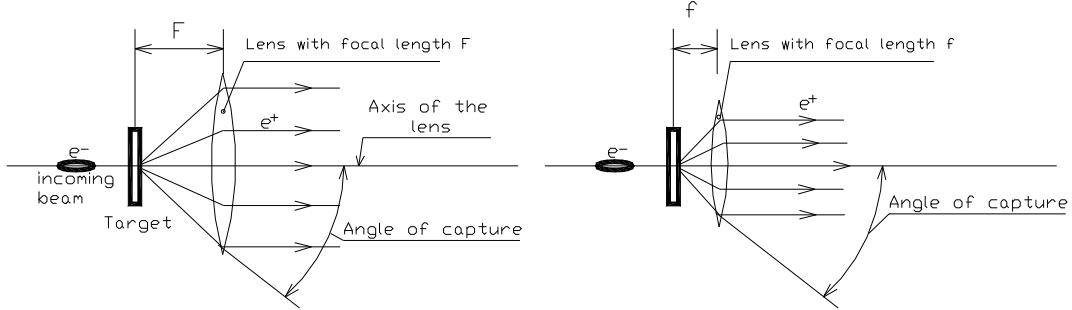
FIGURE 2.1: The geometry of capturing. Target located at the distance F (or f) -the focal distance of the lens. Shorter focal distance–smaller the beam size, as the divergence of the beam remains the same.

Second principle can be illustrated as follows. If the hot spot is off-axis with respect to the focal point of the lens, the secondary beam receives an angle $\alpha \cong \dfrac{x}{F}$, where x is a misalignment, see Fig.2.2.
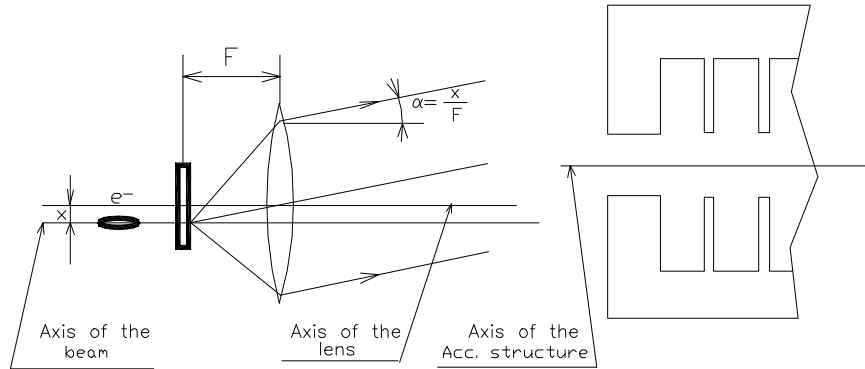
FIGURE 2.2: The beam line and the lens axis have a shift x. All three axes must be congruent.

The focal distance F for the solenoidal type of lens used is given by

$$F = \frac{4(HR)^2}{\int H^2(s)ds},$$ (2.1)

where (HR) is a magnet rigidity of the particle, $pc=300(HR)$, $H(s)$ is a longitudinal field distribution on the axis, s is a longitudinal coordinate. One can see, that the focal distance has a *quadratic* dependence on energy (and on feeding current I, $H \propto I$).

The angle of the plane rotation is $\theta = \int H(s)ds / 2(HR)$. These formulas can be easily obtained after the field consideration in 3D, as

$$H_r(r,s) \cong -\frac{r}{2}\frac{\partial H(s)}{\partial s} + \frac{r^3}{16}\frac{\partial^3 H(s)}{\partial s^3} - ... \quad , \quad H_s(r,s) \cong H(s) - \frac{r^2}{4}\frac{\partial^2 H(s)}{\partial s^2} - ... \quad .$$ (2.2)

The field under an ideal condition of angular symmetry has only longitudinal and radial components. So the angular kick α for fixed mismatch has a quadratic dependence on energy and feeding current in a solenoidal lens as

$$\alpha \cong \frac{x}{F} \cong \frac{x \cdot \int H^2(s)ds}{4(B\rho)^2} \, ,$$

where x –is the transverse offset of the primary beam with respect to the axis of solenoid, Fig. 2.2.

So, this kick is extremely sensitive both to the level and distribution of magnetic field as well as the energy of secondary particles. The misalignments generated by the short focusing solenoid yields a transverse wave downstream. So the losses may occur somewhere in the beginning of the acceleration as well as somewhere downstream.
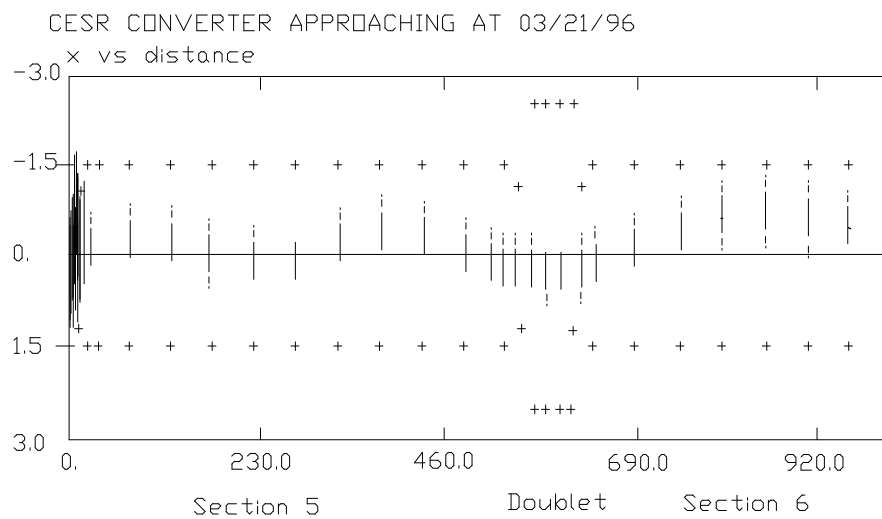
FIGURE 2.3: Transverse misalignment of the beam trajectory in sections 5 and 6. Energy of the positrons is 5*MeV*. Current running in pulsed solenoidal lens 4*kA*, misalignment $\Delta y = 3mm$. Crosses mark aperture limits [5].
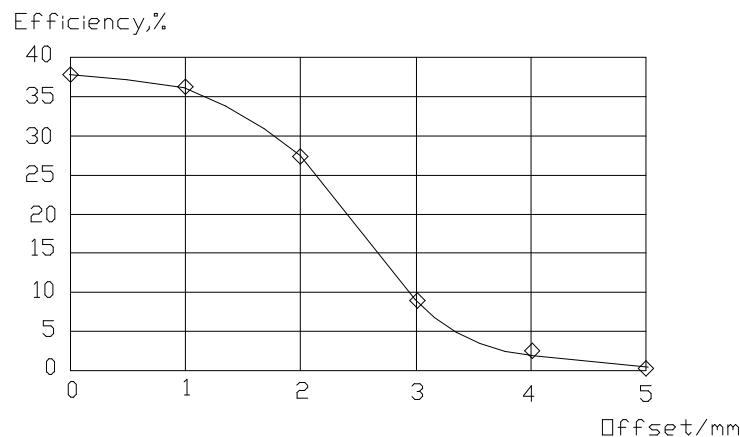

FIGURE 2.4: Efficiency of the capture as a function of misalignment [5].

Third and fourth principles –symmetry in input wires and surroundings are in line of what was just described above. Any of these asymmetries makes it impossible to increase the focusing without

introduction of transverse kick. So the effect of increasing the capturing efficiency becomes diminished by losses generated by kick.

3. COLLECTION OPTICS

Geometry of the modified capturing optics is represented in Fig.3.1. This is pretty much the same as the original one. The only difference is in the focusing coil design. This coil is working in pulsed mode, naturally, as the feeding current required, according to (2.1) can reach a 5 *kA* level.
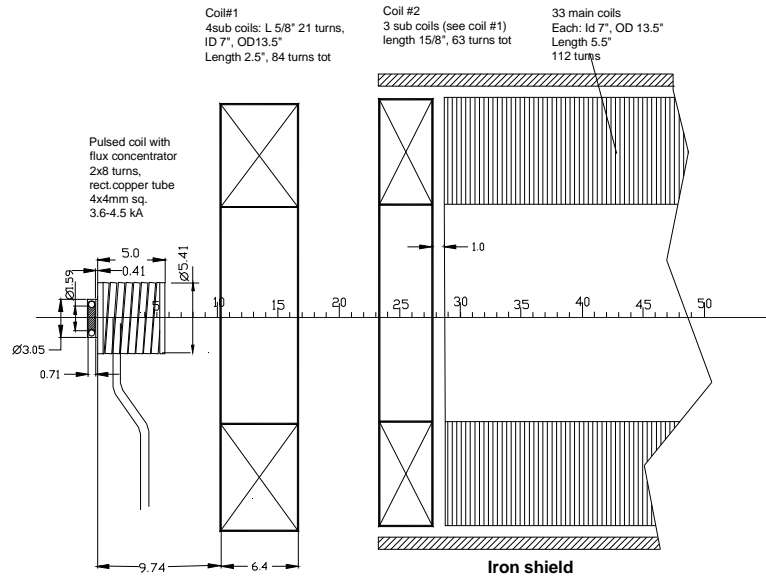
FIGURE 3.1: The converter assembly with focusing solenoid. Primary electron beam is coming from the left.

The face plane of the first coil with large diameter in Fig. 3.1 is located levelly with the input plane of accelerator structure, section #5. In the gap between this first coil and main section of solenoid the input waveguide is squeezed. Saying ahead the current in this first coil for better performance must be zero. Right now this coil is fed in series with the main solenoid.

Target made of an alloy of 97% Tungsten, 2.1% Nickel and 0.9% Iron. Radiation lengths for tungsten W is $X_W \cong 8 \text{g/cm}^2$, geometric length, corresponding to this radiation length, is $LX_W \cong 0.35 \text{cm}$, for Iron $X_{Fe} \sim 13.8 \text{g/cm}^2$, $LX_{Fe} \cong 1.75 \text{cm}$. So the effective radiation length goes as

$$\frac{1}{LX_{eff}} \cong \frac{W_W}{LX_W} + \frac{W_{Fe}}{LX_{Fe}} \cong \frac{0.97}{3.5} + \frac{0.03}{17.5} \cong \frac{1}{3.58}, \tag{3.1}$$

what gives $LX_{eff} \cong 3.58$ *mm*. Optimal thickness of the target has a logarithmic dependence on energy

$$l_{opt} / X_{eff} \cong 1.1 \ln E[GeV] + 3.9. \tag{3.2}$$

For a 200*MeV* primary electron beam (3.2) goes to $l_{opt} \cong 2.12 X_{eff}$, which gives $Ll_{opt} \cong 2.12 X_{eff} \cong 7.59 mm$. We have chosen, however, the thickness of the target $L \cong 7.063 mm$, i.e. a little bit less that what is given by (3.2). The reason for this is a weak dependence of positron

production versus thickness around optimum, see Fig. 3.2. If the target is thinner, there will be fewer problems with heating.

Another important number to remember is the skin depth of the pulsed field in Tungsten, which is around 1 *mm* for the pulse parameters, see below.

Numerical calculations as in [5] were carried out with the PARMELA code. The files with initial positron distributions were generated using results [7]. Here the transverse distribution of the positrons created by an electron at the hot spot is defined as

$$\frac{d^2N^+}{dxd\theta_x} = \frac{1}{\pi\varepsilon_x^+}\exp\{-\frac{\gamma x^2 + 2\alpha x\theta_x + \beta\theta_x^2}{\varepsilon_x^+}\}, \tag{3.3}$$

where emittance is defined as

$$\varepsilon_x^+ = 2\sqrt{<x^2><\theta_x^2> - <x\theta_x>^2}, \quad \gamma = 2<\theta_x^2>/\varepsilon_x^+, \quad \alpha = -2<x\theta_x>/\varepsilon_x^+, \quad \beta = 2<x^2>/\varepsilon_x^+. \tag{3.4}$$

Here x measured as a fraction of the radiation length, i.e. $x = 1$ means, that x equals the length, corresponding the radiation length, which is 3.5 *mm* for Tungsten. The brackets in (3.3) mean to average over the ensemble. Equation $\gamma x^2 + 2\alpha x\theta_x + \beta\theta_x^2 \le \varepsilon_x^+$ describes the phase ellipse with about 63% of the particles in it. The values for different energies and for the target having a thickness of $2X_0$ and an incoming beam with energy $200MeV$ are the following [7]

<div align="right">Table 3.1.</div>

|	$E^+ = 5\ MeV$	$E^+ = 10\ MeV$	$E^+ = 20\ MeV$
$<x^2>$	0.043	0.05	0.032
$<\theta_x^2>$	0.35	0.22	0.12
$<x\theta_x>$	0.025	0.052	0.038
$\varepsilon_x^+ cm\cdot rad$,(3.4)	0.084	0.085	0.034

As the current pulse in the lens lasts for about 25 microseconds (see below), the current induced inside the Tungsten target by the pulsed magnetic field penetrates to a depth about 0.8 *mm*. On the other hand, the RMS depth l of positron creation $l \cong \dfrac{<x\theta_x>}{<\theta_x^2>}$ can be estimated as 0.83 *mm* for 10

MeV positrons. The drop of the magnetic field begins at the distance of the order of the coil radius as a result of the counter-current induced in the target. So one can conclude that the most of the particles are created in very low longitudinal magnetic field. This was modeled by the introduction of image currents as it was done in [5].

The fraction of particles, created with some particular energy can be found from Fig. 3.2 [7], where the spectrum of positrons is represented. This spectrum is calculated for positrons outgoing from the target in solid angle $\Omega = 2\pi$ forward and normalized to a single incoming $200MeV$ electron. The number of the positrons ΔN^+ for different energy interval of captured positrons as a convolution

$$\Delta N^+ = \int_{E\min}^{E\max} F(E^+)\cdot\eta(E^+)\frac{dE^+}{E^+}, \tag{3.5}$$

where the function $F(E^+) = E^+ \dfrac{dN^+}{dE^+}$, represented on Fig. 3.2, and $\eta(E^+)$ is an efficiency of *geometrical* capture for a particular energy.
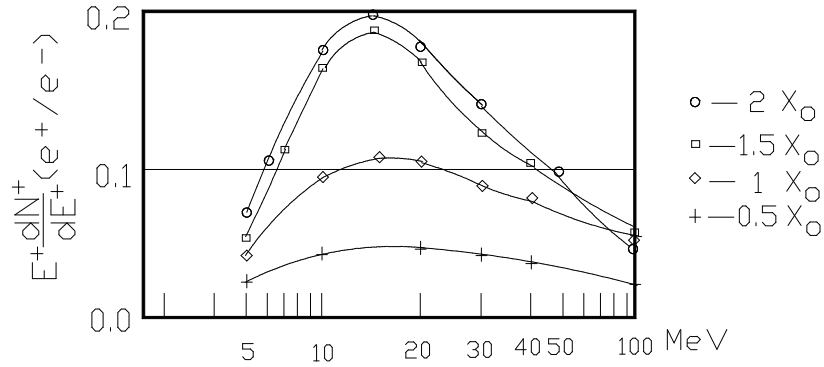
FIGURE 3.2: The spectrum of outgoing positrons for different thickness of the target [5].

E_{min} and E_{max} are defined by energy acceptance of the downstream optics. Maximal positron yield occurs around the critical energy for the Tungsten what is 600/Z~10*MeV*. From Fig. 3.2 we can calculate the average energy of the secondary beam, using

$$< E^+ > \cong \int E^+ \frac{dN^+}{dE^+} dE^+ = \int F(E^+) dE^+ , \tag{3.6}$$

which gives about the same number $< E^+ > \cong 9 MeV$.

For 10 *MeV* positrons geometrical capture efficiency was found to be 40%. So formula (3.5) gives $\Delta N^+_{10} \cong 0.036$ or 3.6% for 10 *MeV*. Real numbers, of coarse will be lower, because of geometrical capture needs to be averaged over the energy interval of captured positrons.

Coil-Concentrator **is** represented in Fig. 3.3 below. It is wound with Oxygen free copper conductor having 4×4 *mm*^{2} square cross section with a water hole of 2.5 *mm* in diameter. It has 16 turns total in two layers.
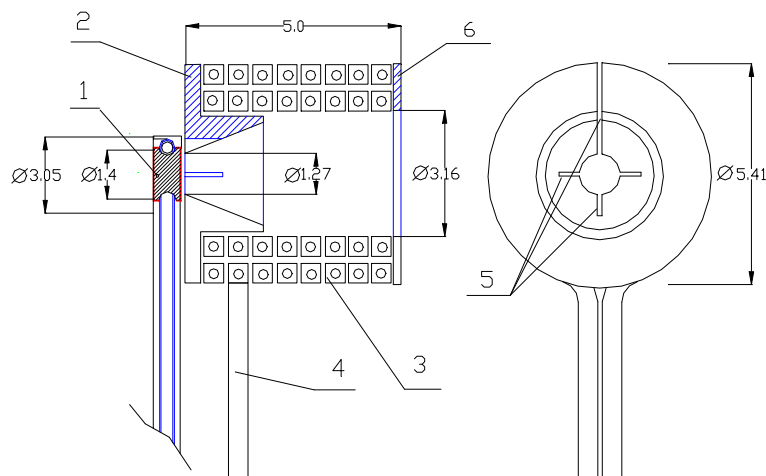

FIGURE 3.3: Scaled view from Fig. 3.1. 1-target, 2-flux concentrator, 3-bilayer solenoid, 4-feeding leads, 5-slots, 6-end plate. Copper conductor has cross section of 4x4 mm^2. Dimensions are given in cm.

The input leads are running in the shadow region of the flux concentrator. For symmetryzation three more semi-slots (5 in Fig.3.3) across the end plate were added.
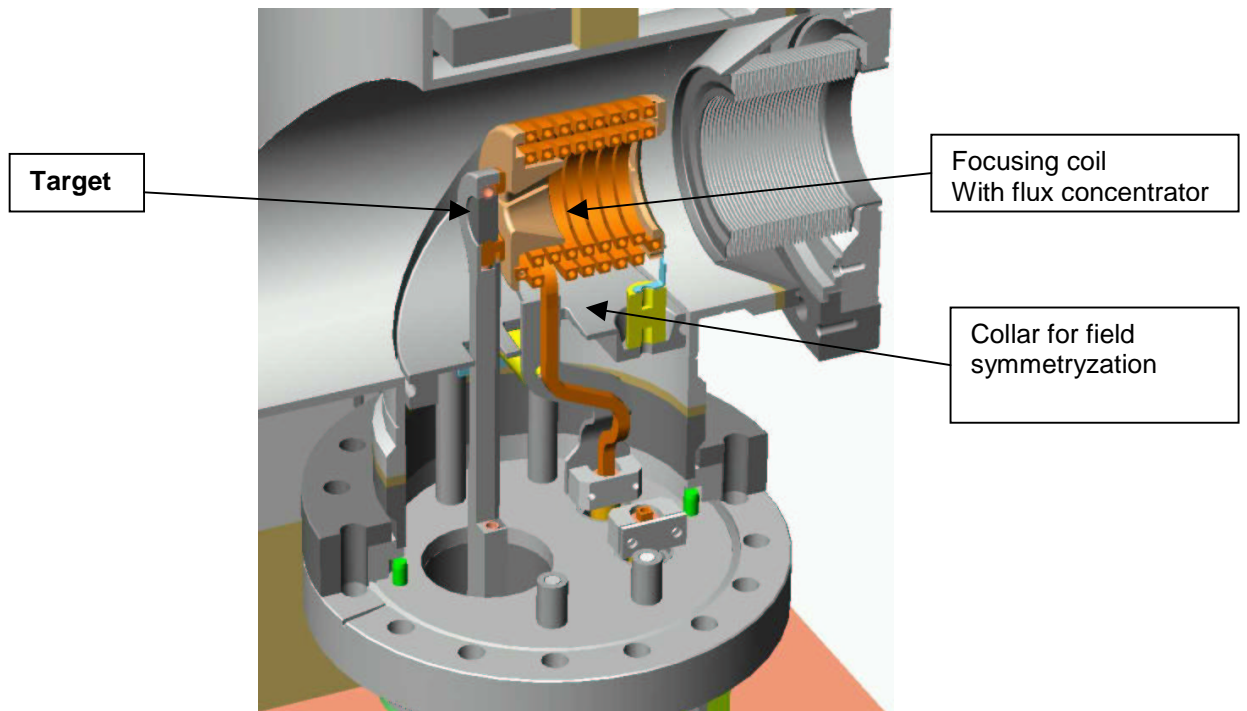
FIGURE 3.4: An isometric view of the focusing coil. The target is fixed at the end of the paddle-type holder.

The housing is made of Aluminum. This drastically reduces the losses from imaginary currents induced in the walls. Really, as the flux is conserved, the field is present between the coil and the wall. So the field has a significant fraction outside of the coil. Calculations show that the field reduction inside the coil due to surrounding walls is about 15% for the size of the tubing.
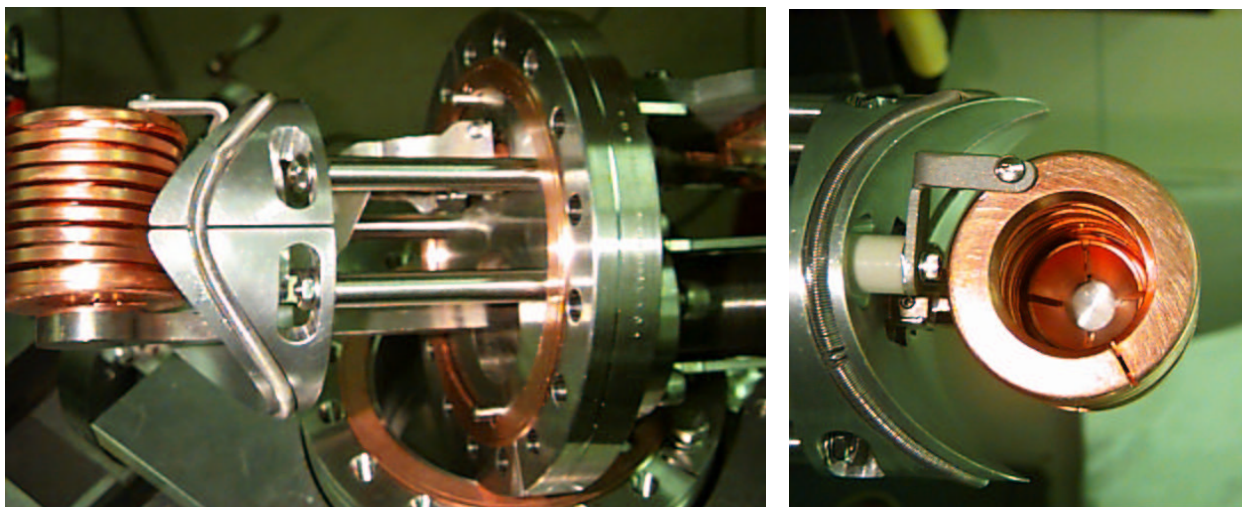
FIGURE 3.5: Photo of the focusing coil and the target.

Special collar like looking detail in Fig. 3.5 makes a continuation of the cylindrical shape around the coil. A helical spring makes a good contact between the part and the rest of the cabinet. Aluminum also reduces accumulation of isotopes.

Measurements were carried out with the same procedure, as described in [4]. The field at maximal point in Fig.3.6 is ~10kG, which is in good agreement with calculation. For calculation of magnetic field the model was used, which takes into account the skin depth of the current in flux concentrator media as well as in the target. For this the imaginary currents were applied running on the surfaces of the flux concentrator and target. After that the currents found are positioned in PARMELA input file[1].
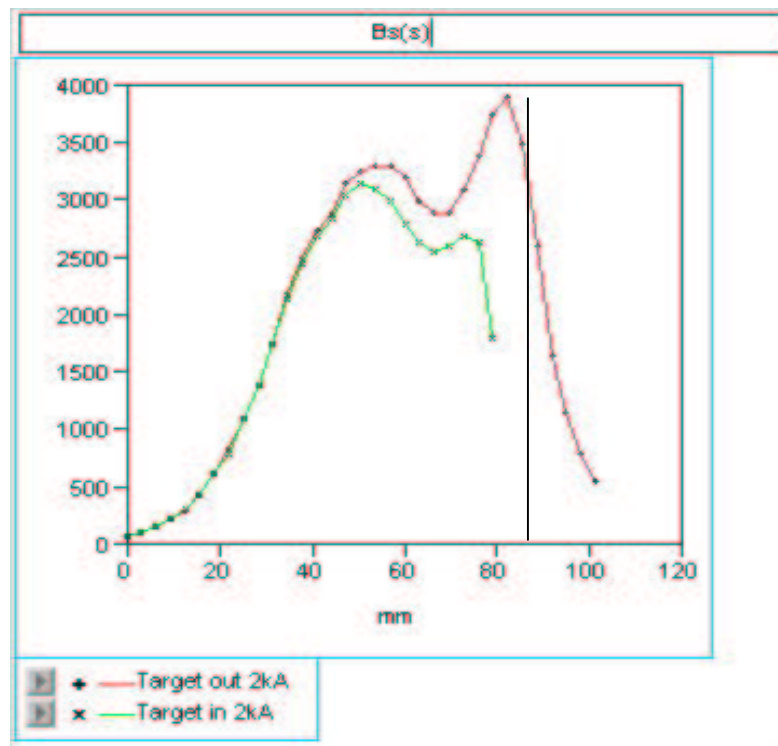
FIGURE 3.6: Longitudinal component of the field as a function of the distance, @2 kA. Peak field here is $\cong$ 10 kG. At the surface of the target this component ~zero. Azimuthal component, indeed, increases. Surface of the target marked by the line. Primary electron beam is coming from the right side of the picture.

Movement of the housing with target and solenoid in the transverse plane to the beam direction arranged with the help of two stepping motors. Fig.3.7. Allowed motion is $\cong \pm 5$ *mm* in each direction.

Strip line made on copper sheets having width 4.2 *in* of outer two plates and 3.75 *in* central plate. Two layers of 10 *mils* Kapton insulate these electrodes. Line still flexible enough allowing motion of the cabinet.

Paddle type holder of the target allows transverse motion of the target for removing it from the beam line during electron injection (as it was in original design).

---

[1] Details will be published.
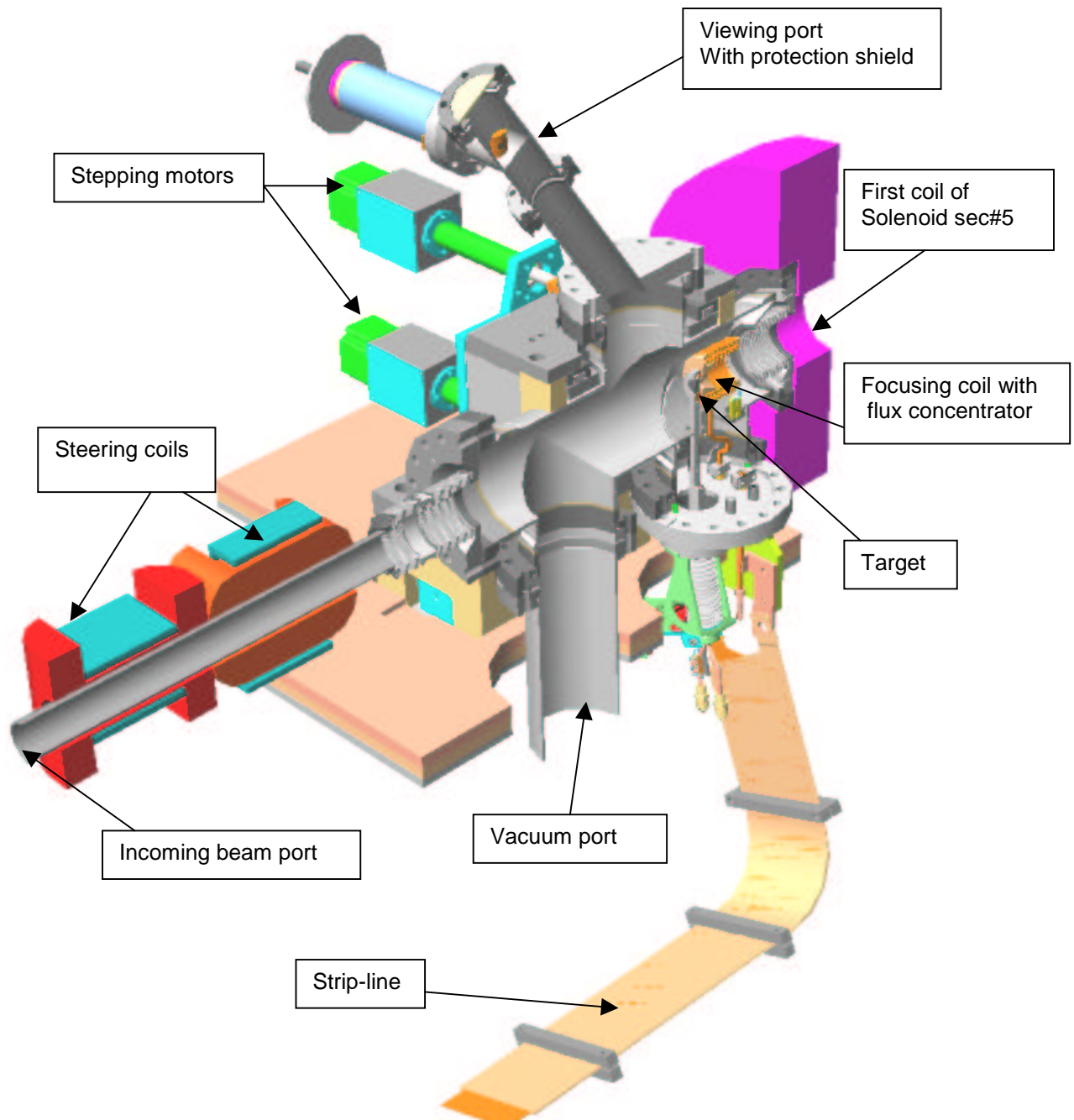
FIGURE 3.7: Converter unit. Focusing triplet located on incoming beam tube right before steering coils shown here and other viewing port (not shown in this figure).

4. PULSER UNIT

The pulsed power supply was redesigned for higher current capabilities and more reliability. We implemented *modular* concept for power supply. Principal scheme of power supply is represented in Fig. 4.1. Equivalent scheme of the pulser is represented in Fig. 4.2.

The transfer line from the pulser to the lens made as a wide strip-line and partly with ten coaxial cables in parallel for flexible attachment to the pulser. The pulser tested for a long time period with modified lens at current ~4.6 *kA* and shortly for 5 *kA*.
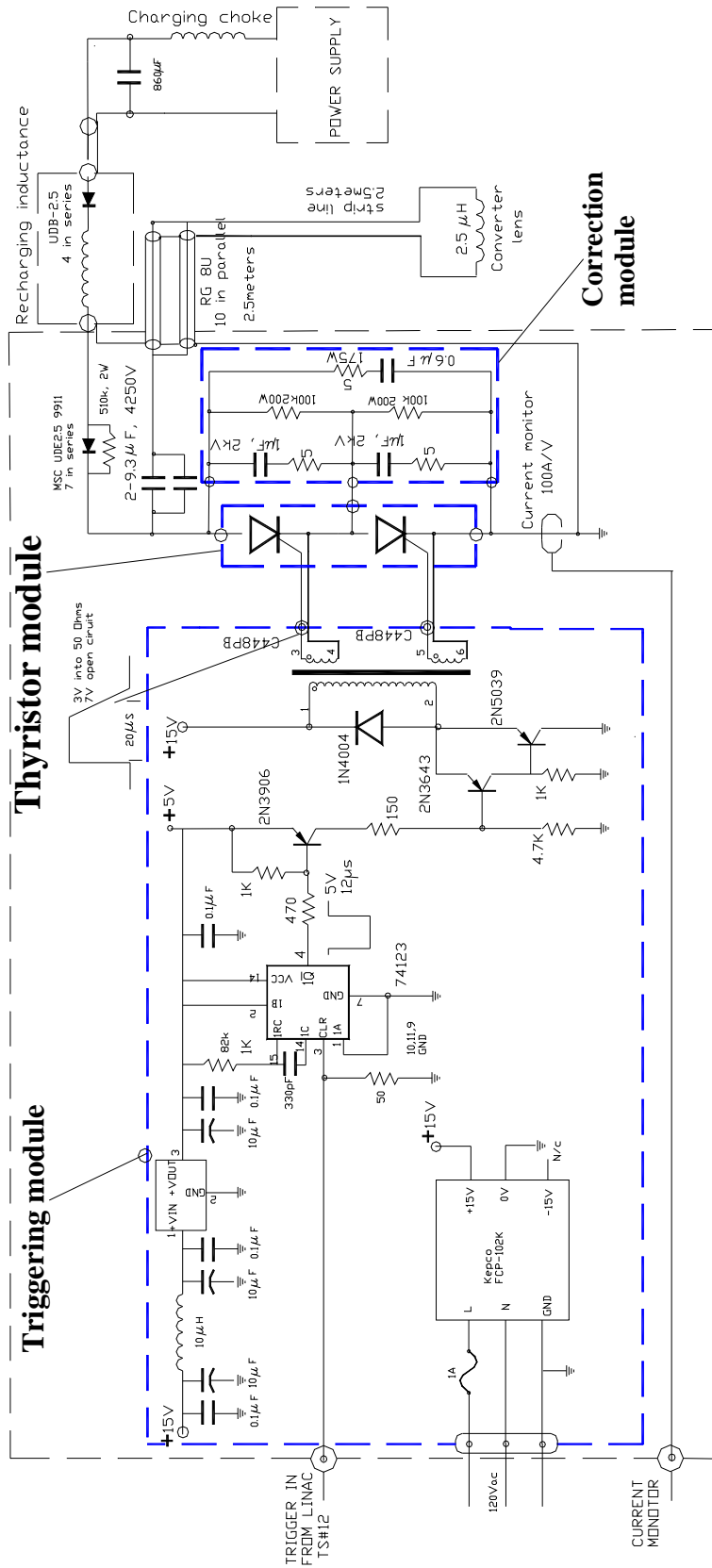
FIGURE 4.1: The pulser. Ready chains are not shown. Modular design allows easy replacement of triggering and thyristor modules.

Formally the scheme looks similar to what was used before with one critical difference however. We recognized importance of having large capacitor C (in Fig. 4.2) and charging it with *constant current*. This procedure drastically reduces the losses allowing work with low charging voltage.
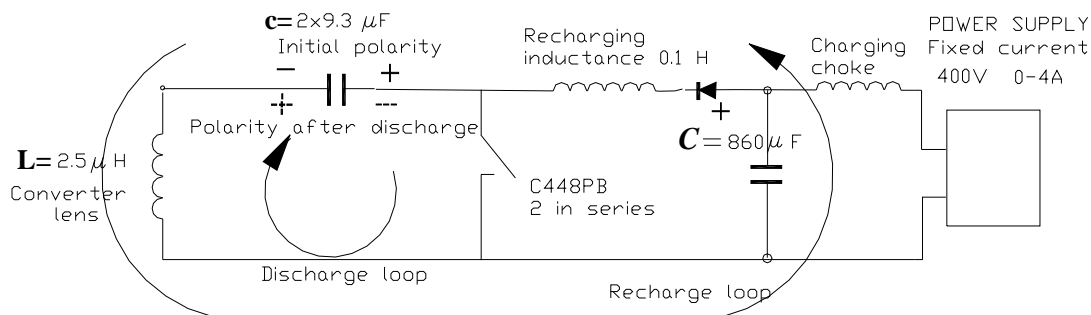
FIGURE 4.2: Equivalent scheme. The voltage hold on capacity of the power supply is adding to the recharging voltage every time during recharging. Power supply is charging capacity with *constant* (fixed) current.

Capacitor c in Fig. 4.2 is a part of discharge loop together with the inductance of the lens. After thyristors C448PB are triggered, the current is going through the inductance L until the polarity of voltage on capacitor c reverses its sign. This is the discharge phase. As the current through the thyristors ceases, which is the end of discharge, recharge stage begins. Recharging loop includes the same elements: inductance of the lens L, capacitor c plus additional recharging inductance and capacitor C. One can see in Fig. 4.2, as the capacity $C \gg c$, the voltage held on capacitor C by power supply, is added to the initial voltage held on c minus losses in the chains. Capacitor C is charged by power supply in fixed current mode. The final voltage on c is established after a few oscillations. Typically the voltage at capacitor c four times higher than that provided by power supply. For voltage on PS set to the level ~315 *V*, average current with this voltage goes to 4.4 *A* and pulsed current goes to ~4 *kA*.

In Fig. 4.3 the thyristor module is shown. This module was made to be easy removable. Basically it is connected with the motherboard by three bolts. One spare module (two in total) allows guaranteed operation and fast replacement. The housing allows easy access to the joint bolts. Fast replacement time reduces the exposure time for personnel.
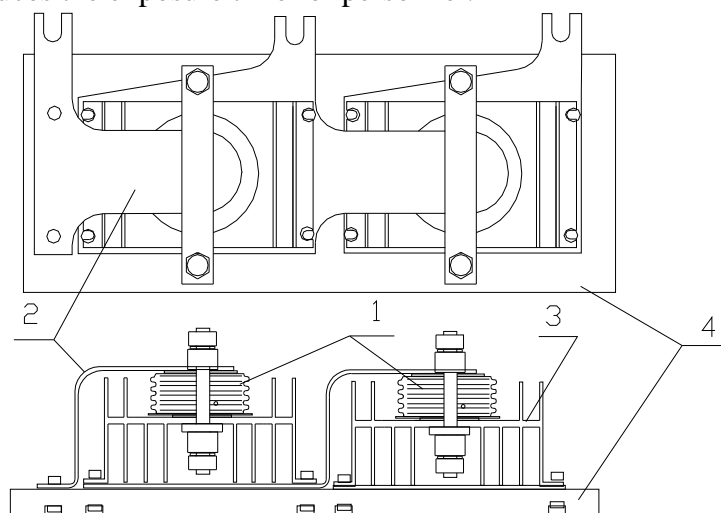
FIGURE 4.3: Thyristors' module. 1–thyristors, 2– the metallic plate-conductors, 3– a heat sink, 4– a G10 base.

Special attention is paid for reduction of inductance. The plate caring thyristors has a grounded metallic base for these purposes.
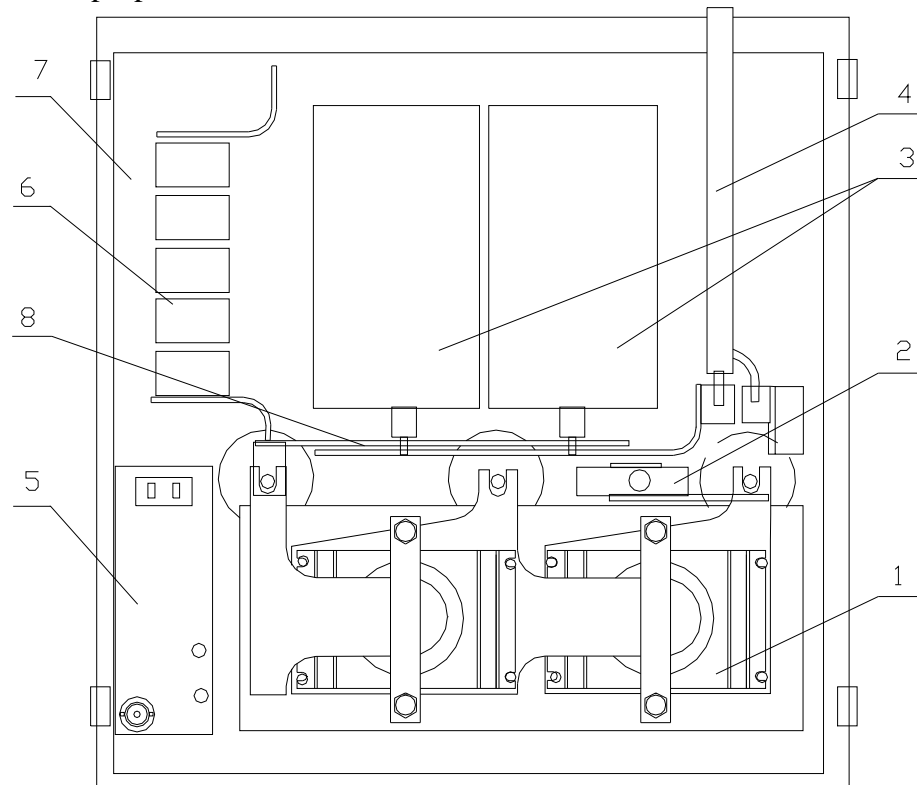

FIGURE 4.4: Structure scheme of the pulser. 1-the switch module from previous Figure. 3-capacitors *c*, 2-Rogowsky-type current monitor, 4-coaxial line, 5-triggering module, 6-diods, 7-metallic plate-basement, 8-wide inter conductors.

FIGURE 4.5: Pulser (left) and power supply with interlocks (right). RMS 600-8-2-D from LAMBDA EMI is used as a power supply.

Inner plate can be easily rolled off the cabinet for repair and checking.
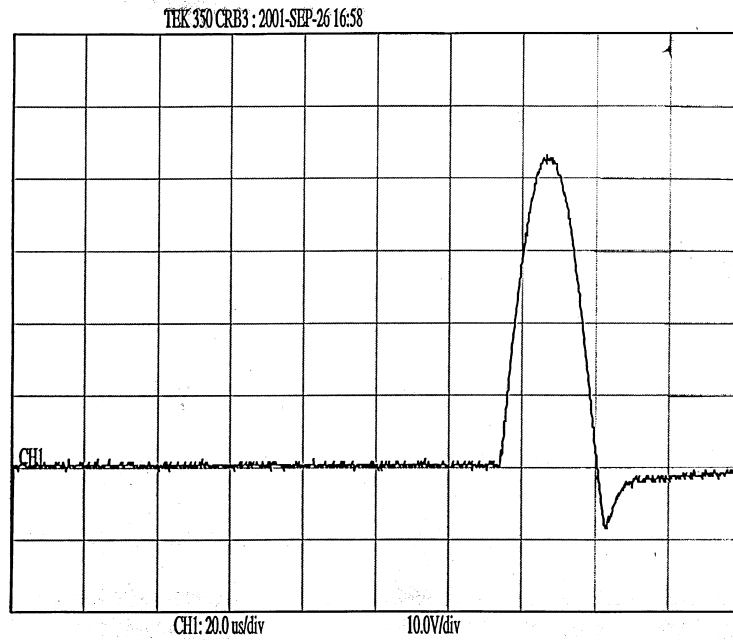
FIGURE 4.6: Signal from the current monitor read in control room. Horizontal scale 20 μs /division. Vertical scale– 1kA/div.

Signal read in control room from shunt is represented in Fig. 4.6. Duty time over basement of the pulse is ~27 μs .

5. INSTALLATION INTO LINAC/TUNING RESULTS

Pulser installed closer to the target area in front of protection shield near section #4.
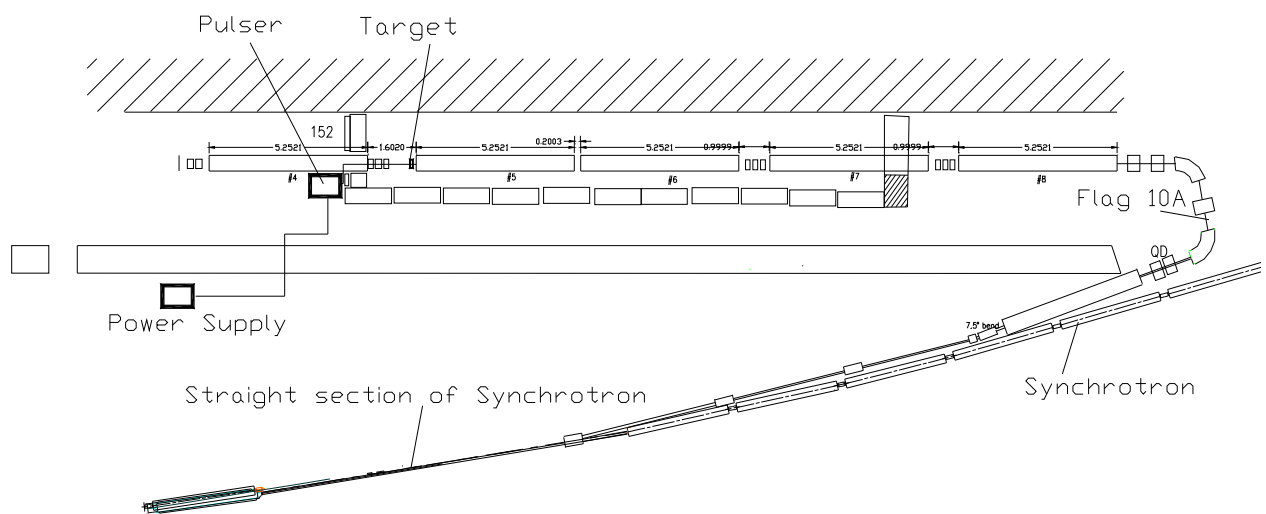
FIGURE 5.1: Positron channel map. Pulser installed near target area behind the concrete wall.

FIGURE 5.2: Pulser unit located in front of the converter cave. Section #4 is located at the left, behind the lead shield. Electron beam is running from the left side of the picture.
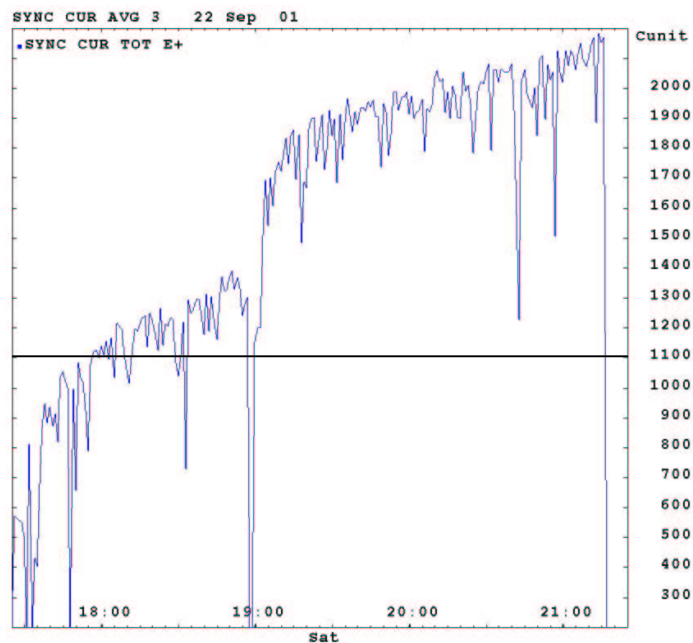
FIGURE 5.3: Tuning progress during the first run. Single bunch. Line marks previous achievements.

Right now even without any fine tuning the rate of accumulation of positrons in CESR is ~110*mA/min*.

6. POSSIBLE IMPROVEMENTS

The points for further improvements are:

- Calculations carried with PARMELA code indicate that the efficiency can be increased up to 15% with first coil (#1 in Fig.3.1) off. See also Fig. 3.7.
- Current can be risen up to 4.5 *kA* as the system was tested at this level. This might increase the capture up to 60%. Right now the pulsed current is kept at the level of 3.6 *kA* just for allowing CESR tunings without extremes.
- Possible installation of the focusing element(s) before the target. Right now the primary electron beam is focused on the target with the help of triplet assembled as a unit block. The midplane of this triplet located at $\cong 120cm$ apart from the target. The steering coils mostly (one for each direction) occupy the space between the triplet and the converted housing, see Fig. 3.7.

A Lithium lens as well as a set of short focusing quadrupoles can be installed closer to the target. Really, the enlargement of primary beam in a target could be estimated as

$$\sigma_\perp \approx t \cdot \sqrt{<\theta^2>} \cong t \cdot \frac{13.6 MeV}{pc} \sqrt{t_{Xo}/X_{eff}} \ , \tag{6.1}$$

where X_{eff} –is an effective radiation length of the target, t –is the thickness of the target in *cm*, t_{Xo} –is the thickness of the target in *g/cm²*. For ~200 *MeV* primary electron beam and Tungsten target the transverse size of bunch enlargement will be $\sigma_\perp \cong 0.7 \cdot \frac{13.6}{200} \sqrt{2} \cong 0.06cm$, or 0.6 *mm*. As the photons created after one X_{eff} passed, the last estimation can be reduced by $\sqrt{2}$ and goes to $0.5mm$.

We mentioned also that the effective depth l of positron creation is $l \cong \frac{<x\theta_x>}{<\theta_x^2>}$. For 10 *MeV* positrons this was estimated as 0.83 *mm*. According to (6.1) the RMS size of secondary positron beam goes to $\sigma_\perp \approx 0.55mm$.

So two processes: enlarging of primary electron beam and secondary positron beam due to multi scattering process gives the RMS positron size of the order $\sigma_{rms} \cong \sqrt{0.25+0.3} \cong 0.74mm$.

This number gives estimation to the maximal geometrical value of desirable beam size of the primary beam. Now this size is about 2.5*mm*. So there is evident necessity to decrease the size of the beam irradiating the target. This can increase the phase density of the positron beam as much as three times.

Limit for the material of target destruction under illumination by the bunch with population *N* can be taken from experimental work done at SLAC as [8]

$$NE/\pi\sigma^2 \cong 2 \cdot 10^{12} GeV/mm^2 . \tag{6.2}$$

Here the *NE* is total energy carried by the bunch. The targets of optimal thickness supposed to be in use for every particular energy. We have $\sim 20nC/pulse$ or $\sim 1.25 \cdot 10^{11}$ electrons, which yields $\sigma \geq 10^{-6}\sqrt{NE/2\pi} \cong 0.06mm$. So the primary beam size can be reduced more than 40 times.

Additional focusing by Lithium lens for example can do this lowering of the primary beam spot size. The short focusing triplet can be also used here. ***Anyway existing triplet located too far from the target.***

As *the cheapest solution* we recommend to move triplet closer to the target on the place of steering coils. Steering coils can be moved in position occupied by triplet now or implemented into quadrupole yoke.

• Let us estimate the maximal possible energy interval, allowed by the optics of the transfer line and energy compressor, see Fig. 5.1. The analyzer magnets (region around flag 10A in figure 5.1) have a bending radius $\rho \cong 85 cm$ and the path length of the beam line $l \cong 108.5 cm$. This gives a bending angle $\varphi = l / \rho \cong 1.27 rad$. So, the difference in the path length for the particles, having energy spread ΔE^+ around some average energy E_0^+ will be (for two magnets)

$$\Delta l \cong 2 \cdot \rho \cdot (\varphi - Sin\varphi)\Delta E^+ / E^+.$$

This difference must be within the half wavelength of the energy compressor (or, may be, a little more), i.e. $\Delta l \cong \lambda / 2 \cong 5 cm$. Supposing $E_0^+ \cong 150 MeV$ (after acceleration), one can obtain that $\Delta E^+ \leq 15 MeV$. At the end of the first analyzer magnet the dispersion will be $\eta \cong \rho \cdot (1 - Cos\varphi) \approx 0.7\rho \cong 60 cm$ and its derivative will be $\eta' \cong Sin\varphi \cong 0.95$. So, in the middle of the straight section between two magnets having 2 m distance, (flag 10A), the dispersion will be $\eta_{center} \cong \eta + \eta' \cdot L \approx 150 cm$, where we supposed that the $L \approx 1m$. So for the energy spread 10%, this gives the beam radial dimension on flag 10A about $\pm 7.5 cm$. One can see that one of the restrictions for beam transport may occur here.

7. CONCLUSION

Modifications of the positron converter unit done so far gave the basis for further increase of CESR's luminosity. Possible items for more additional improvements are indicated also.

8. REFERENCES

[1] M. Billing, N. Kazarinov, *The possibility of Increasing the positron Production for CESR Injection*, CBN 93-5, Cornell 1993.
[2] V. Anosov, M. Billing, D. Kaltchev, V. Kazacha, N. Kazarinov, A. Krasnykh, E. Perelstein, M. Tigner, A. Vasilenko, *Electron-Positron High-Efficiency Converter*, Preprint JINR, E9-95-403, Dubna, 1995.
[3] V. Alexandrov, A. Mikhailichenko, *Positron Beam Capture and Acceleration*, CON95-23.
[4] A. Mikhailichenko, *Field distribution around QWT and Converter*, CON96-15, August 14, 1996.
[5] A. Mikhailichenko, *To the Positron Collection at CESR Complex*, CON97-01, February 4, 1997
[6] G. Stange, *A pulsed Magnetic Lens for Positron Focusing: numerical calculations and first measurements with a prototype,* DESY S1-73/4, August 1973.
[7] V.A. Tajursky, *Calculation of Electron Conversion into Positrons at 0.2—2GeV*, BudkerINP 76-36, Novosibirsk, 1976.
[8] S. Ecklund, *Positron Target Materials Tests*, SLAC-CN-128, 1981.